

# Prediction of Building Integrated Photovoltaic Cell Temperatures

By

Mark W. Davis , Brian P. Dougherty,  
and A. Hunter Fanney

National Institute of Standards and Technology  
Building and Fire Research Laboratory  
Heat Transfer and  
Alternative Energy Systems Group  
Gaithersburg, MD 20899-8632 USA

Reprinted from Transactions of the ASME, the Journal of  
Solar Energy Engineering, Special Issue: Solar  
Thermochemical Processing, Vol. 123, No.2, pp. 200-210,  
August 2001.

NOTE: This paper is a contribution of the National  
Institute of Standards and Technology and is not subject to  
copyright.

# Prediction of Building Integrated Photovoltaic Cell Temperatures\*

*A barrier to the widespread application of building integrated photovoltaics (BIPV) is the lack of validated predictive performance tools. Architects and building owners need these tools in order to determine if the potential energy savings realized from building integrated photovoltaics justifies the additional capital expenditure. The National Institute of Standards and Technology (NIST) seeks to provide high quality experimental data that can be used to develop and validate these predictive performance tools. The temperature of a photovoltaic module affects its electrical output characteristics and efficiency. Traditionally, the temperature of solar cells has been characterized using the nominal operating cell temperature (NOCT), which can be used in conjunction with a calculation procedure to predict the module's temperature for various environmental conditions. The NOCT procedure provides a representative prediction of the cell temperature, specifically for the ubiquitous rack-mounted installation. The procedure estimates the cell temperature based on the ambient temperature and the solar irradiance. It makes the approximation that the overall heat loss coefficient is constant. In other words, the temperature difference between the panel and the environment is linearly related to the heat flux on the panels (solar irradiance). The heat transfer characteristics of a rack-mounted PV module and a BIPV module can be quite different. The manner in which the module is installed within the building envelope influences the cell's operating temperature. Unlike rack-mounted modules, the two sides of the modules may be subjected to significantly different environmental conditions. This paper presents a new technique to compute the operating temperature of cells within building integrated photovoltaic modules using a one-dimensional transient heat transfer model. The resulting predictions are compared to measured BIPV cell temperatures for two single crystalline BIPV panels (one insulated panel and one uninsulated panel). Finally, the results are compared to predictions using the NOCT technique. [DOI: 10.1115/1.1385825]*

**Mark W. Davis**

e-mail: mark.davis@nist.gov

**A. Hunter Fanney**

e-mail: hunter@nist.gov

**Brian P. Dougherty**

e-mail: brian.dougherty@nist.gov

National Institute of Standards and Technology,  
Heat Transfer and Alternative Energy  
Systems Group,  
100 Bureau Dr. STOP 8632,  
Gaithersburg, MD 20899-8632

## Introduction

Building integrated photovoltaic (BIPV) products are drawing more attention from the building industry as the price of photovoltaic modules continues to drop [1]. The Building and Fire Research Laboratory at the National Institute of Standards and Technology (NIST) seeks to facilitate informed decisions on when and how to effectively deploy BIPV products. NIST contributes by providing high quality experimental data, which is used to develop, validate, and refine computer simulation tools.

The prediction of the photovoltaic module's cell temperature plays an important role in the modeling of its electrical and thermal performance. The cell temperature depends on many physical and environmental factors. The construction of the module and the manner in which it is installed in the building influence its operating temperature. Environmental conditions, such as the ambient temperature, solar irradiance, wind speed, and wind direction also affect the cell temperature.

The nominal operating cell temperature (NOCT) is commonly used to predict the cell temperature over a range of environmental conditions. By definition, the NOCT is the temperature of the cells at a solar irradiance of 800 W/m<sup>2</sup>, an ambient temperature of 20°C, and a wind speed of 1 m/s. The American Society for Testing and Materials (ASTM) has developed a standard method to determine the NOCT (E 1036M Annex A1) [2].

The NOCT approach is based on the more common scenario where both sides of the PV module *see* the same ambient tem-

perature and wind conditions. Notably, the approach also makes the approximation that the overall heat transfer coefficient for the PV module is constant.

Understandably, when a PV module is integrated into the exterior envelope of a building, the potential for deviating from the heat transfer case captured by the NOCT model is substantial. For example, the two sides of the building integrated module will typically be subjected to significantly different environmental conditions. The heat transfer, and ultimately the PV cell operating temperature, is affected by the building mounting mechanism. Insulating materials, if installed on the interior side of the building and BIPV module, add to the potential deviations. Additionally, if the manufacturer's NOCT value is used in lieu of a temperature more representative of the panel's insulation level, errors will result in the predicted cell temperature. Therefore, the method used for determining the cell temperature must accurately cover a wide range of environmental conditions and mounting arrangements.

With these possible deviations in mind, NIST made some initial comparisons of NOCT predicted cell temperatures versus measured BIPV cell temperatures. These initial comparisons suggested, as expected, that the NOCT approach has limitations when used for predicting BIPV cell temperatures. Efforts were then made to develop predictive methods that were tailored to BIPV applications. The proposed methods, their basis, and initial comparison with measured data, are the focus of this paper. Comparisons with the NOCT approach are provided.

## Approach

Measured BIPV cell temperatures are available from NIST's Building Integrated Photovoltaic *test bed*. The *test bed* includes eight instrumented BIPV panels that are mounted vertically in the south wall of the Building and Fire Research Laboratory on the

\*This paper was presented at Forum 2001, *Solar Energy: The Power To Choose*, April 21–25, 2001, in Washington DC.

Contributed by the Solar Energy Division of the THE AMERICAN SOCIETY OF MECHANICAL ENGINEERS for publication in the ASME JOURNAL OF SOLAR ENERGY ENGINEERING. Manuscript received by the ASME Solar Energy Division, November, 2000; final revision March, 2001. Associate Editor: C. Vargas-Abruto.

NIST campus in Gaithersburg, Maryland. The NIST BIPV *test bed* also incorporates a small weather station on the building façade [3].

Four cell technologies are presently featured in the NIST BIPV *test bed*: single crystalline, polycrystalline, silicon film, and triple-junction amorphous silicon. Two panels of each technology are installed. One panel of each cell type is insulated with extruded polystyrene that has a measured thermal resistance of 3.46 m<sup>2</sup>·K/W, whereas the other panel is installed without insulation. Three out of the four pairs of panels were custom fabricated. The single crystalline, polycrystalline, and silicon film panels consist of a Tedlar<sup>2</sup>-Mylar<sup>2</sup> backsheets, the respective cell technology, and a 6 mm thick piece of solar glass. Individual amorphous silicon cells were not available for fabricating a custom sized building integrated photovoltaic panel. Thus, commercially available triple junction amorphous silicon modules were used. A complete description of the panels is included in a paper presenting initial results from the test facility [4].

This paper focuses on the thermal and electrical performance of the two single crystalline panels. Temperature measurements for each of the panels are made directly on the back of the panel and on the back of the thermal insulation (where applicable). Thermocouples are attached to the rear of selected cells within the panels. At this time, more than 12 months of data are available for comparison. For the same time frame, the following environmental parameters have been recorded: the indoor and outdoor ambient temperature; wind speed and direction at the panels and on the roof; horizontal and in-plane total solar irradiance; normal incident beam irradiance; and radiative temperature of the indoor and outdoor surroundings. The uncertainty associated with each of these measurements is discussed in Appendix A. This data can be used to predict the cell temperature using the NOCT method and a one-dimensional, transient heat transfer model.

The one-dimensional heat transfer model was formulated to provide a more complex and precise temperature model for BIPV panels. One goal of this paper is to evaluate the benefits of a more complex temperature model as compared to the two-parameter NOCT model.

In any decision concerning BIPV, the amount of power generated is the most important consideration. The prediction of cell temperatures will lead to a comparison of the predicted peak power at each predicted temperature. The calculation of the power produced by a panel was performed on a virtual single crystalline module using a model proposed by Sandia National Laboratories (SNL) [5]. Because not all of the necessary parameters for this model have been measured on the NIST BIPV panels, a module using the same cells as the single crystalline panel was selected from a database of SNL measurements. The power was calculated for this panel using the measured temperature, the temperature predicted using the NOCT technique, and the temperature predicted using the one-dimensional model developed in this paper.

## Model Development

**NOCT Model.** The method for predicting the cell temperature using the nominal operating cell temperature is outlined in ASTM standard E1036M Annex A1 [2]. The nominal operating cell temperature of a panel is measured with the panel in an open rack at a fixed position throughout the day. The panel is positioned at an elevation and azimuth that is normal to the sun at solar noon. The panel temperatures, ambient temperature, total irradiance in the plane of the panel, and wind speed are all measured for an eight-hour period. The standard assumes that the overall heat transfer coefficient is constant, which dictates that the difference between the cell temperature and the ambient tempera-

ture is linearly related to the solar irradiance. Therefore, a line relating the temperature difference to the irradiance is fit to the data, and the NOCT value is interpreted as the temperature difference at 800 W/m<sup>2</sup> according to the fit plus the nominal 20°C ambient temperature. Finally, the average measured ambient temperature and average measured wind speed are used to adjust the NOCT value. The cell temperature at any irradiance level and ambient temperature is determined using [6]:

$$T_{\text{cell}} = \frac{G}{G_{\text{NOCT}}} (\text{NOCT} - T_{\text{ambient,NOCT}}) \cdot \left( 1 - \frac{\eta_c}{\tau\alpha} \right) + T_{\text{ambient}} \quad (1)$$

where

$$G_{\text{NOCT}} = 800 \text{ W/m}^2, \quad T_{\text{ambient,NOCT}} = 20^\circ\text{C}.$$

In this paper, the NOCT values are taken from the manufacturer's specifications [7]. For a rack-mounted panel, the specified NOCT is 45°C. NOCT tests were run on a panel similar to the single crystalline panel. The panel was fabricated the same way as the single crystalline panel, but it utilized polycrystalline cells. The NOCT value for that panel was 44°C. The transmittance-absorptance product was assumed to be the product of the cell absorptance at normal incidence and the glass transmittance at normal incidence.

The irradiance for the NOCT method is measured in the plane of the panel. When these measurements are not available, transformations of horizontal irradiance measurements are necessary. A comparison of the performance of the NOCT model will be made between the irradiance measured in the plane of the panel and irradiance transformed from horizontal measurements.

**One-dimensional Transient Heat Transfer Model.** The NIST proposed alternative method for predicting the cell temperature of a BIPV panel is based on the approximation of one-dimensional, transient heat transfer. This method was also used by a group of researchers attempting to predict the temperature of a PV array on the Martian surface [8]. Their study divided a rack-mounted panel into three layers: the top cover, PV cells, and back layer. The thermal analysis associated with the Martian photovoltaic panel included forced convection from the front surface; natural convection from the rear surface; radiation from the front surface to the sky and the ground; and radiation from the rear surface to the sky, ground, and shaded ground.

The NIST BIPV single crystalline panels are also modeled as multi-layer composites. The layers include the protective cover glass, the PV cells, the backsheets, and the insulation behind the panel on the insulated panel. The physical parameters used in the model are shown in Table 1. The cover glass specifications were obtained from the manufacturer. The thermal and physical properties of the PV cells were assumed to be those of pure silicon, but the nominal thickness of the cells was obtained from manufacturer specifications. Panel efficiencies were measured over the modeled period for the two BIPV panels. The thermal resistance and thickness of the extruded polystyrene insulation were obtained from nominal measurements. The specific heat and density were assumed to be equal to that for generic extruded polystyrene. For the backsheets, the specific heat and density were taken directly from the manufacturer's specification sheet, the thickness was measured from a sample, and the thermal conductivity was estimated from similar polymer films.

The model assumes that the absorbed incident solar radiation not converted to electricity is converted to thermal energy at the cell. This thermal energy is conveyed to the panel surfaces via conduction, and at each surface, convection and radiation transfer heat to the surroundings. A graphical representation of the model can be seen in Fig. 1. The model is described by Eqs. (2)–(8).

$$q''_{\text{solar}} = q''_{\text{out,conv}} + q''_{\text{out,rad}} + q''_{\text{in,conv}} + q''_{\text{in,rad}} + q''_{\text{st}} \quad (2)$$

$$q''_{\text{solar}} = G_{\text{effective}} \cdot (\alpha - \eta_c) \quad (3)$$

$$q''_{\text{out,conv}} = \bar{h}_{\text{out}} \cdot (T_{\text{s,out}} - T_{\text{ambient}}) \quad (4)$$

<sup>2</sup>Certain trade names and company products are mentioned in the text or identified in an illustration in order to adequately specify the experimental procedure and equipment used. In no case does such an identification imply recommendation or endorsement by the National Institute of Standards and Technology, nor does it imply that the products are necessarily the best available for the purpose.

**Table 1 Variables and parameters for one-dimensional heat transfer model**

Layer	Parameter (Units)	Value
Panel	H (m)	1.0
Panel	W (m)	1.2
Panel	$\eta_{uninsulated} / \eta_{insulated}$	0.112/0.107
Cover Material	L (m) [9]	0.006
Cover Material	$\rho$ (kg/m <sup>3</sup> ) [9]	2500
Cover Material	$C_p$ (J/kg·K) [9]	835
Cover Material	$k$ (W/m·K) [9]	1.04
Cover Material	$\varepsilon$ [9]	0.84
PV Cell	L (m) [10]	0.0003
PV Cell	$\rho$ (kg/m <sup>3</sup> ) [11]	1650
PV Cell	$C_p$ (J/kg·K) [11]	700
PV Cell	$k$ (W/m·K) [11]	150
PV Cell	$\alpha$ [12]	0.95
Backsheet	L (m)	0.00017
Backsheet	$\rho$ (kg/m <sup>3</sup> ) [13,14]	1475
Backsheet	$C_p$ (J/kg·K) [13,14]	1130
Backsheet	$k$ (W/m·K)	0.14
Backsheet	$\varepsilon$	0.893
Insulation	L (m) [4]	0.1016
Insulation	$\rho$ (kg/m <sup>3</sup> ) [11]	55
Insulation	$C_p$ (J/kg·K) [11]	1210
Insulation	$k$ (W/m·K) [4]	0.0294
Insulation	$\varepsilon$ [11]	0.9

$$q''_{out,rad} = \varepsilon_{glass} \cdot \sigma \cdot (T_{s,out}^4 - T_{surr}^4) \quad (5)$$

$$q''_{in,conv} = \bar{h}_{in} \cdot (T_{s,in} - T_{indoor}) \quad (6)$$

$$q''_{in,rad} = \varepsilon_{in} \cdot \sigma \cdot (T_{s,in}^4 - T_{surr,indoor}^4) \quad (7)$$

$$q''_{st} = \sum \left( c_{p,i} \cdot \rho_i \cdot L_i \cdot \frac{T_i(t) - T_i(t - \Delta t)}{\Delta t} \right) \quad (8)$$

**Solar Heat Flux.** The solar incident energy that is converted to heat is determined from the beam irradiance, total irradiance, transmittance of the cover glass, absorption of the PV cells, and panel electrical conversion efficiency. The beam and total irradiance are measured with a normal incidence pyrheliometer (NIP) and a pyranometer, respectively. The total irradiance is measured with both a roof and wall mounted pyranometer. These quantities are used to calculate the diffuse irradiance, using Eq. (9). The

effective irradiance,  $G_{effective}$ , equals the amount of total irradiance that reaches the cell surface. Equation (10) shows the procedure used to convert the beam and diffuse irradiance into the effective irradiance using the transmittance of the front cover material. The electrical conversion efficiencies of the BIPV panels, Table 1, were computed from measurements of the electrical energy produced by the panels and the incident solar insolation over the modeled period (August 22 through October 6, 2000).

$$G_{diffuse} = G_{total} - G_{beam,NIP} \cdot \cos(\theta) \quad (9)$$

$$G_{effective} = G_{beam,NIP} \cdot \cos(\theta) \cdot \tau(\theta) + G_{diffuse} \cdot (60^\circ) \quad (10)$$

For the model proposed by NIST, the transmittance of the cover material, glass, for diffuse light is assumed to be the beam transmittance at an incident angle of 60 degrees, 82.6%. The transmittance function is shown in Eqs. (11)–(14) [6].

$$\tau(\theta) = \frac{1}{2} \left( \frac{1 - r_{perpendicular}}{1 + r_{perpendicular}} + \frac{1 - r_{parallel}}{1 + r_{parallel}} \right) \quad (11)$$

$$r_{perpendicular} = \frac{\sin^2(\theta_2 - \theta)}{\sin^2(\theta_2 + \theta)} \quad (12)$$

$$r_{parallel} = \frac{\tan^2(\theta_2 - \theta)}{\tan^2(\theta_2 + \theta)} \quad (13)$$

$$\theta_2 = \sin^{-1} \left( \frac{\sin(\theta)}{n} \right) \quad (14)$$

where  $n = 1.5995$ , which corresponds to the refractive index that results in a normal transmittance equal to the glass manufacturer's reported value of 89.8% [7].

According to Parretta [10], the reflectance for a single crystalline solar cell with an inverted pyramidal texture and an anti-reflective coating varies from 2% to 10% over the applicable range of wavelengths at low incident angles. Therefore, assuming a reflectance of 5% and 0% transmission, the absorptance of the cell would be 0.95.

**Outside Convective Heat Flux.** The convective heat transfer from the cover glass to the outdoor ambient environment is assumed to be dominated by forced convection. The average heat transfer coefficient is determined from the average Nusselt number using

$$\bar{h}_o = \frac{\bar{Nu}_w \cdot k_{air}}{W} \quad (15)$$

The forced convection heat transfer is determined to be laminar. For all panels tested, the critical velocity for laminar flow is 6.2 m/s (13.9 mph), and only five of 13250 wind speed measurements over the modeling period were greater than 5 m/s (11.2 mph). The effective length in this calculation was taken to be the width of the panel. This assumes that the wind currents flow horizontally across the panel. Two applicable Nusselt number relations, Table 2, were compared to determine the formulation that best described the convective heat transfer for the panels.

**Radiative Heat Flux.** Radiation heat transfer occurs between the outside cover glass and the surroundings and between the backside of the insulated or uninsulated BIPV panel and the indoor environment. The effective temperature of the surroundings in Eqs. (5) and (7) are determined from infrared radiation measurements and the relationship,

$$T_{surr} = \left( \frac{q''_{PIR}}{\sigma} \right)^{1/4} \quad (16)$$

**Inside Convective Heat Flux.** It is assumed that the convective heat transfer from the backside of the panel (or insulation) to the indoor ambient conditions is dominated by natural convection.

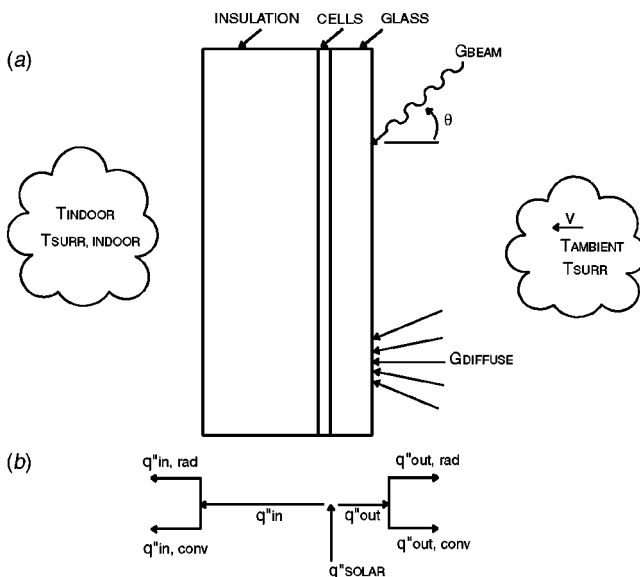


**Fig. 1 a) cross-sectional view of panel installation, and b) a nodal representation of heat flux of the one-dimensional heat transfer model**

**Table 2 Forced convection relations for the average Nusselt number over the panel**

ID Number	Name	Nusselt Relation	Conditions
1	Constant Temperature [11]	$0.664 Re_L^{1/2} \cdot Pr^{1/3}$	Laminar flow, uniform surface temperature, $Pr > 0.6$
2	Sparrow et al. [6]	$0.86 Re_{Lc}^{1/2} \cdot Pr^{1/3}$	$20000 < Re_{Lc} < 90000$ , $L_c = \frac{4 \cdot A_{panel}}{P}$

**Table 3 Natural convection relations for the average Nusselt number over the panel**

ID Number	Name	Nusselt Relation	Conditions
1	Ostrach [15]	$0.476 \cdot Gr_L^{1/4}$	Laminar flow, $Pr = 0.72$ , uniform surface temperature
2	Ede [15]	$\left[ \frac{0.4 \cdot Pr}{1 + 2 \cdot Pr^{1/2} + 2 \cdot Pr} \right]^{1/4} \cdot Gr_L^{1/4} Pr^{1/4}$	Laminar flow, uniform surface temperature
3	Integral Solution [15]	$0.677 \cdot \left( \frac{Pr^2}{0.952 + Pr} \right) Gr_L^{1/4}$	Laminar flow, uniform surface temperature
4	LeFevre [11]	$\frac{0.7071 \cdot Gr^{1/4} \cdot Pr^{1/2}}{(0.609 + 1.221 \cdot Pr^{1/2} + 1.238 \cdot Pr)^{1/4}}$	Laminar flow, uniform surface temperature

**Table 4 Assumptions made in model proposed by NIST for the four different model variations**

Model	Assumptions
1	None
2	$T_{surr} = T_{ambient}$ , $T_{surr,indoor} = T_{indoor}$
3	$T_{surr} = T_{ambient}$ , $T_{surr,indoor} = T_{indoor}$ , $V_{wall} = V_{roof}$
4	$T_{surr} = T_{ambient}$ , $T_{surr,indoor} = T_{indoor}$ , $V_{wall} = V_{roof}$ , $G = f(G_{horizontal})$

Similar to forced convection, the average indoor heat transfer coefficient, Eq. (17) was determined by the average Nusselt number for the indoor conditions.

$$\bar{h}_{in} = \frac{\bar{Nu}_H \cdot k_{air}}{H} \quad (17)$$

Four applicable Nusselt number relations were compared for natural convection, Table 3. Unlike the outside convective heat flux, the air currents on the inside surface of the panel were assumed to flow vertically. Thus, the height of the panel was used as the effective length in this calculation. The natural convection was also assumed to be laminar. For laminar natural convection on a 1 m high vertical panel, the critical temperature difference between the backside of the panel and the indoor environment is approximately 13°C. For the dataset considered, less than 15% of the uninsulated panel measurements exceeded 13°C. All of the insulated panel measurements were well below the 13°C temperature difference.

*Change in Stored Energy.* The change in stored energy from one time step to the next is calculated according to Eq. (8). The temperature change of each material is affected by its specific heat, thermal conductivity, mass (shown as density and thickness), and the length of time between steps. The stored energy term is a significant advancement over the NOCT model. Accounting for thermal mass prevents unrealistic swings in calculated panel temperatures during periods of quickly changing irradiance levels.

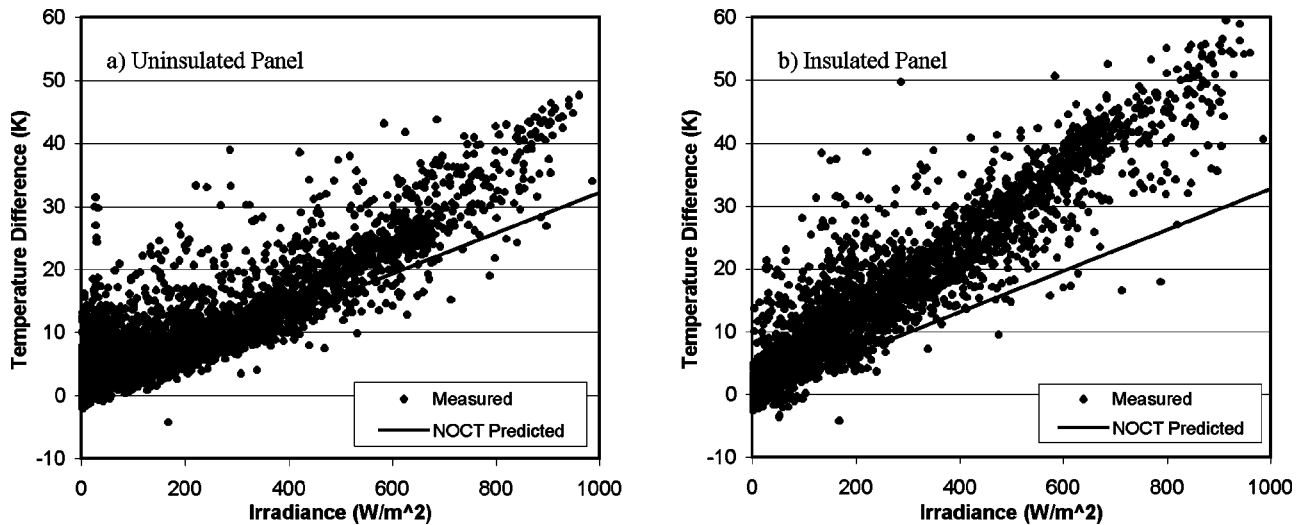


**Fig. 2 Measured temperature difference between an (a) uninsulated and (b) insulated panel compared to the NOCT predicted temperature difference**

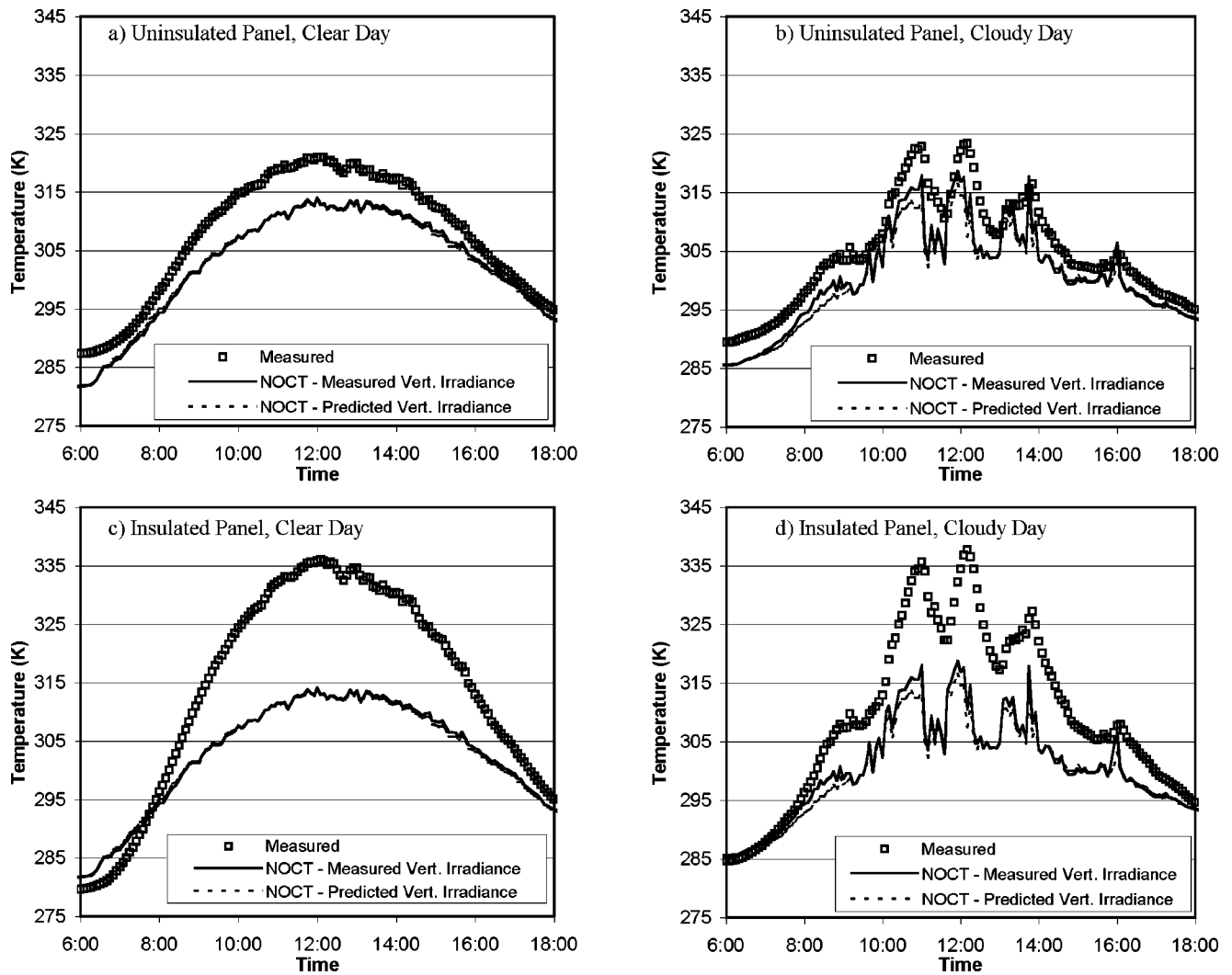


**Fig. 3 Measured and NOCT model predicted panel temperatures (measured vertical and estimated vertical irradiance) for an (a) uninsulated panel on a clear day, an (b) uninsulated panel on a cloudy day, an (c) insulated panel on a clear day, and an (d) insulated panel on a cloudy day**

**Variations of Heat Transfer Model.** The model described above may require measurements that are not readily available to architects while designing a building. Therefore, variations of the original model, denoted as Model 1, were considered. Simplifying assumptions result in heat transfer models that most architects can readily use. The minimum amount of climatic information required to use the most simplified model is outlined below:

- Outdoor ambient temperature data
- Wind velocity data
- Horizontal total irradiance and normal incident beam irradiance data
- Indoor ambient temperature data

Table 4 shows the assumptions for each model variation. The first variation on the original model, Model 2, assumes that the effective temperatures of the surroundings are equivalent to the respective indoor and outdoor temperatures. Model 3 is a variation on Model 2, and it assumes that the wind speed across the panel is equal to the wind speed in the free stream. In our case, a rooftop anemometer measures the free stream wind speed. Finally, Model 4 uses radiation measurements in the horizontal plane and transforms them to the plane of the panels.

The transformation of measured horizontal radiation to that on a vertical façade assumes an anisotropic sky [6]. A true aniso-

tropic sky model includes a term for horizon brightening. For the NIST BIPV test bed, an adjacent building blocks the horizon from view of the BIPV panels. Therefore, the horizon brightening term is assumed to have a negligible effect on the total tilted irradiance. The NIP, which has an aperture of  $5.7^\circ$ , measures the circumsolar diffuse radiation term of the anisotropic sky model along with the beam radiation. Equations (18), (19), (20), and (21) convert total horizontal, normal incident beam, and horizontal diffuse radiation to total radiation on a surface tilted at an angle,  $\beta$ .

$$G_{\text{Diffuse,Hor}} = G_{\text{Total,Horizontal}} - G_{\text{Beam,NIP}} \cdot \cos(\text{Zenith}) \quad (18)$$

**Table 5 R<sup>2</sup> values for NOCT panel temperature prediction using both the measured and estimated irradiance on a vertical surface**

Insulation Level	R <sup>2</sup> Value	
	Measured Vertical Irradiance	Predicted Vertical Irradiance
None	0.77	0.70
R-20	0.49	0.45
Both	0.58	0.54

**Table 6 Predicted energy (kWh) and the percent difference from the predicted energy using the measured panel temperature for each panel on both a clear and cloudy day**

Source of Panel Temperatures	Uninsulated Panel Clear Day		Uninsulated Panel Cloudy Day		Insulated Panel Clear Day		Insulated Panel Cloudy Day	
	kWh	% Diff	kWh	% Diff	kWh	% Diff	kWh	% Diff
Measured	0.296	—	0.191	—	0.277	—	0.182	—
NOCT-Measured Vertical Irradiance	0.307	3.6	0.196	2.5	0.307	10.6	0.196	7.7
NOCT-Predicted Vertical Irradiance	0.304	2.6	0.173	-9.6	0.304	9.6	0.173	-5.0

$$G_{\text{Beam}} = G_{\text{Beam,NIP}} \cdot \cos(\theta) \quad (19)$$

$$G_{\text{Diffuse}} = G_{\text{Diffuse,Hor}} \cdot \left( \frac{1 + \cos(\beta)}{2} \right) + G_{\text{Total,Hor}} \cdot \rho_g \cdot \left( \frac{1 - \cos(\beta)}{2} \right) \quad (20)$$

$$G_{\text{effective}} = G_{\text{Beam}} \cdot \tau(\theta) + G_{\text{Diffuse}} \cdot \tau(60^\circ) \quad (21)$$

The ground reflectance,  $\rho_g$ , in Eq. (20) was determined to have an approximate value of 0.15. A large percentage of the surfaces in front of the BIPV test bed are asphalt, and asphalt has a reflectance of approximately 15% [16] over a range of wavelengths from 400 nm to 1200 nm, which corresponds to the spectral response of the cells [10].

### Model Solution

The prediction of panel temperatures using the NOCT method is straightforward. However, the one-dimensional transient heat transfer model results in a set of non-linear, non-homogeneous differential equations, and it requires an iterative solution. An implicit finite difference scheme was used to solve the model. Each layer (cover material, cells, backsheet, and insulation) was divided into four sections. Nodes were placed at the center of each section. Additionally, a section of zero thickness was placed on indoor and outdoor surface of the panel assembly to facilitate the comparison of predicted and measured temperatures. The equations were solved in matrix form, but due to the nonlinear nature of the model, iteration of the surface temperatures was required.

### Results and Discussion

The results presented for both the NOCT and one-dimensional heat transfer model utilize the correlation coefficient,  $R^2$ , to quantify the success of the temperature prediction. The  $R^2$  values are calculated for times when the total irradiance was greater than zero (and power is generated). The one-dimensional transient model was run at five-minute intervals over the period between August 22, 2000 and October 6, 2000, which includes a mix of clear, partly cloudy, and overcast days.

**NOCT Model.** According to the NOCT technique, the temperature difference between the PV cells and the outdoor ambient conditions is strictly a linear function of the irradiance. Therefore, a plot of the temperature difference between the PV cell and the outdoor ambient temperature as a function of irradiance, as seen in Figs. 2(a) and (b), is linear. This figure includes nine months of temperature data for the panels recorded in the BIPV test bed, which includes a wide range of ambient temperatures and incident angles. The large amount of scatter is caused by many factors. First, the thermal storage capacity of the panels can lead to high temperature differences coupled with low irradiance values on partly cloudy days. Second, variations in wind speed, which drive the forced convective cooling on the outside panel surface, result in significant changes in panel temperatures. This effect is more pronounced at higher values of solar irradiance due to the elevated temperatures of the panel.

The uninsulated single crystalline panel temperature, predicted by the NOCT technique, Fig. 2(a), shows that the measured temperature differences can deviate 10 K or more from the NOCT

prediction. The insulated panel temperature is not predicted well by the NOCT technique at high irradiance values, Fig. 2(b). At an irradiance of 600 W/m<sup>2</sup>, the NOCT technique underpredicted the panel temperature by approximately 20 K.

Figures 3(a)–(d) compare NOCT predictions of uninsulated and insulated single crystalline panel temperatures for a representative clear (September 17, 2000) and partly cloudy day (September 18, 2000). These plots reiterate the significant underprediction of panel temperatures when using the NOCT model for insulated panels and to a lesser degree for the uninsulated panels. The NOCT model more accurately estimates the uninsulated single crystalline panel temperatures. The deviation from the actual temperature at 12:00 hours on the typical clear day is approximately 10 K, Fig. 3(a), in contrast to a 20 K difference for the insulated panel, Fig. 3(c). The larger deviation of the insulated panels is expected considering that the NOCT temperatures, in accordance with ASTM E 1036M, are measured on uninsulated panels. Also, because the NOCT model only depends on the irradiance and the ambient temperature, the predicted panel temperature for the in-

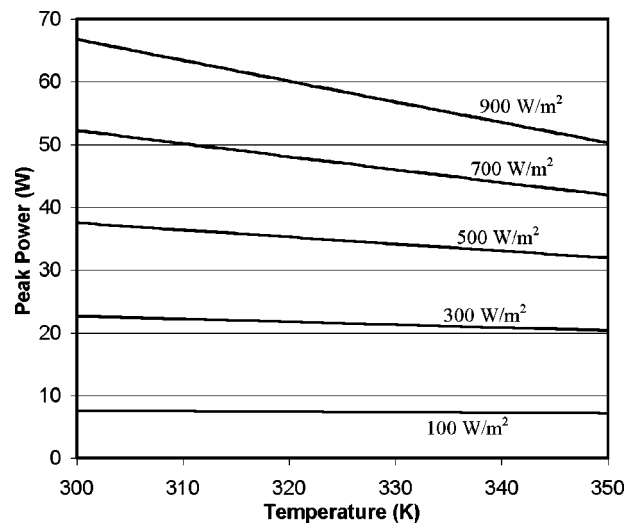


**Fig. 4 Peak power vs. cell temperature and total irradiance for virtual single crystalline cell as calculated by Sandia National Laboratory Model**

**Table 7 Predicted energy production over the modeled period using temperatures predicted with the NOCT model for both the measured and estimated irradiance on a vertical surface**

Insulation	Source of Temperatures for Power Model		
	Measured (kWh)	NOCT Model	
		Measured Vertical Irradiance (kWh)	Predicted Vertical Irradiance (kWh)
None	8.40	8.63	7.77
R-20	7.93	8.63	7.77

**Table 8** R<sup>2</sup> values for all combinations of convection relations

Forced Conv. #	Natural Convection Relation Number			
	1	2	3	4
1	0.9451	0.9427	0.9456	0.9449
2	<b>0.9721</b>	0.9666	0.9720	0.9720

**Table 9** R<sup>2</sup> comparison of model variations between each panel

Insulation Level	Temperature Model				
	1	2	3	4	NOCT
None	0.98	0.98	0.97	0.92	0.77
R-20	0.97	0.93	0.98	0.94	0.49
Both	0.97	0.95	0.98	0.94	0.58

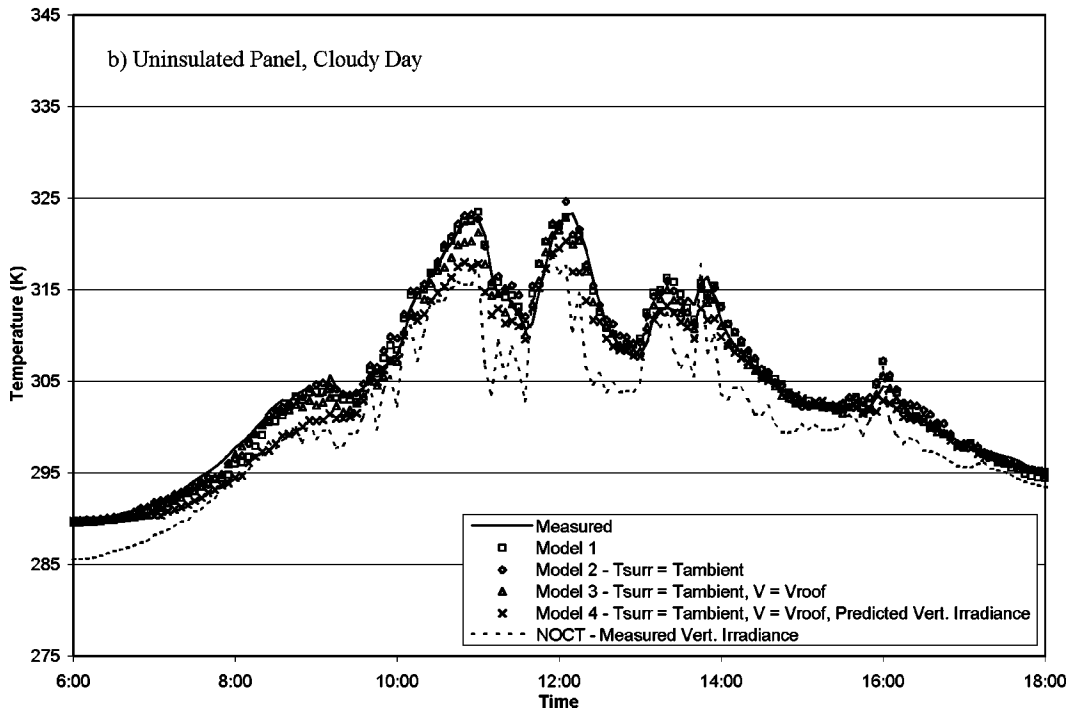
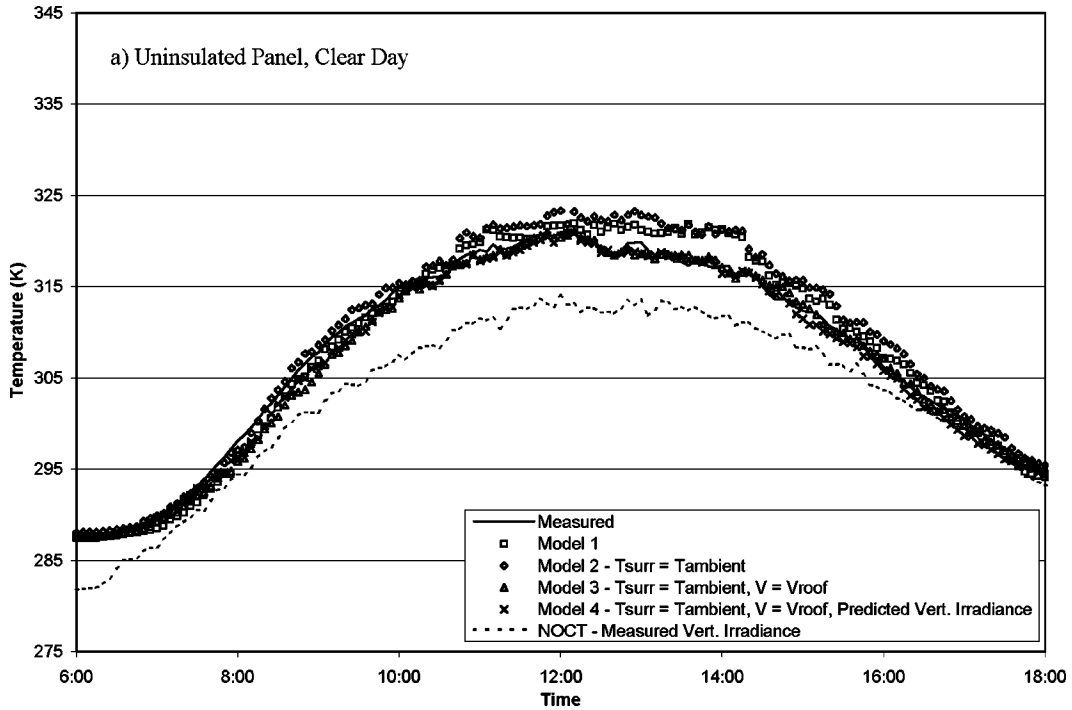


**Fig. 5** Measured and predicted uninsulated panel temperatures for Models 1–4 for a (a) clear day and a (b) cloudy day

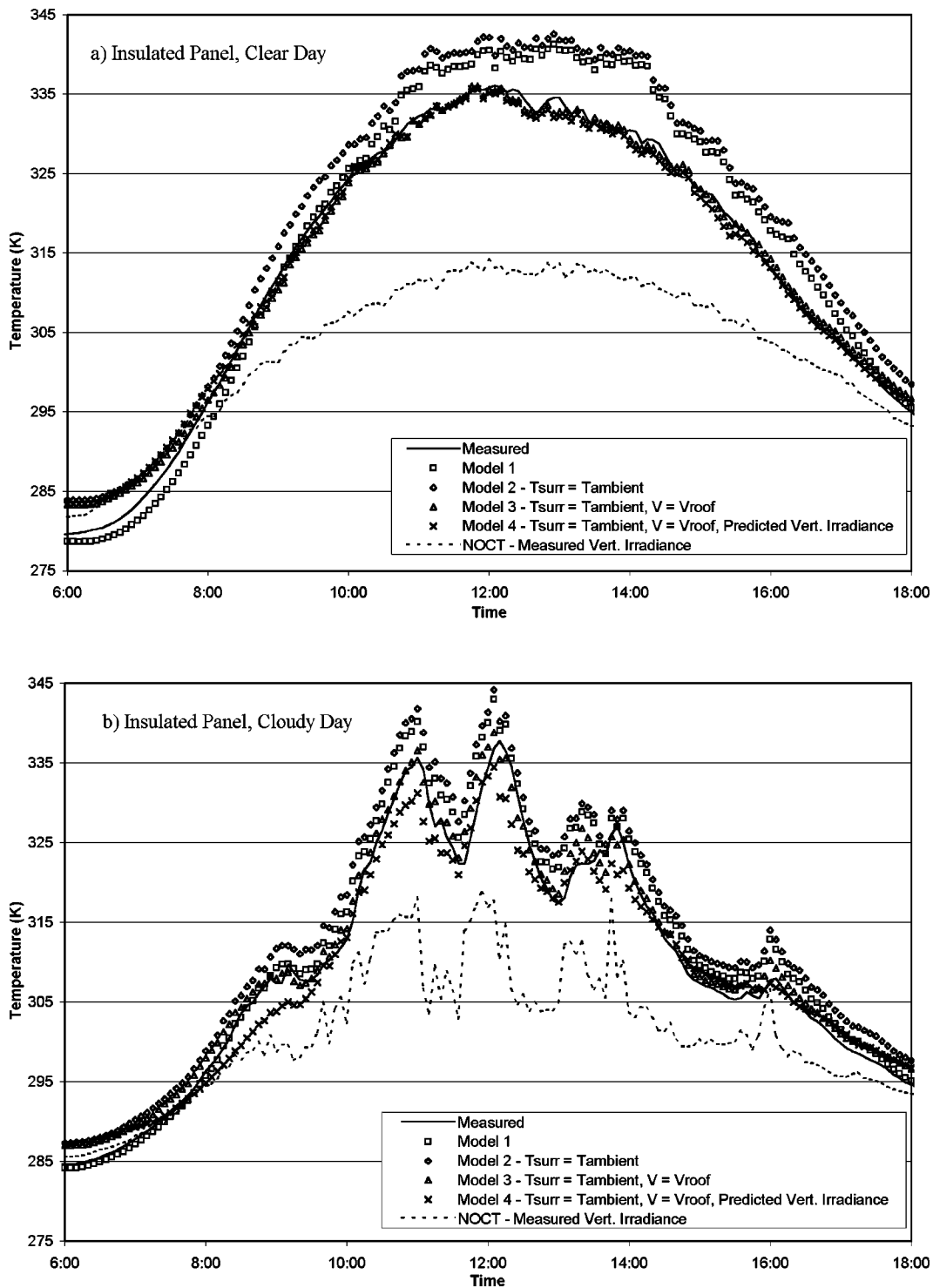


**Fig. 6** Measured and predicted insulated panel temperatures for Models 1–4 for a (a) clear day and a (b) cloudy day

insulated and uninsulated panels are equal. Table 5 shows  $R^2$  values for the two panels using both the measured vertical irradiance and the predicted vertical irradiance, Eqs. (18)–(21).

Table 6 demonstrates the large deviation in the predicted electrical power of an uninsulated and insulated single crystalline panel for both a clear and cloudy day. As stated earlier, the peak power was predicted using the various measured and estimated panel temperatures in a model proposed by Sandia National Laboratory [5]. The NOCT model using the transformed horizontal irradiance results in a power prediction that is slightly different on

cloudy days than the NOCT model using the measured vertical irradiance. This difference results from the small difference between the two irradiance values. A small difference in the irradiance makes a large difference in the power. Figure 4 illustrates the change in predicted peak power as a function of panel temperature. The peak power can differ greatly within a 20 K window at higher values of irradiance. Table 7 shows the energy production predicted using the actual panel temperatures and using the panel temperatures predicted by the NOCT model for the entire modeled period.

**Table 10 Comparison of predicted total energy production over the modeled period using measured temperatures and temperatures predicted by model 1-4**

Insulation	Source of Temperatures for Power Model				
	Measured (kWh)	Model (kWh)			
		1	2	3	4
None	8.40	8.40	8.37	8.46	7.63
R-20	7.93	7.78	7.69	7.96	7.24

**One-Dimensional Heat Transfer Model.** The original one-dimensional transient heat transfer model, Model 1, was expected to more accurately and precisely predict panel temperatures as compared to the NOCT model. Four variations of the model were run over the same data set to investigate the benefits of increasing model complexity. First, convection relations for the inside and outside surfaces were chosen.

*Forced and Natural Convection Relations.* All eight combinations of the applicable forced and natural relations, Tables 2 and 3, were run on the same data set. A composite value of  $R^2$  for both panels was computed for each convection relation combination, which gave a quantitative measure of the accuracy of each combination. Table 8 lists the  $R^2$  values for each combination of convection relations. The convection relation numbers for both forced and natural convection reference Tables 2 and 3, respectively. The **bolded** entry in Table 8, (forced convection relation 2, natural convection relation 1), was chosen as the best set because it resulted in the highest  $R^2$  value. The Sparrow correlation, forced convection relation 2, and the Ostrach relation, natural convection relation 1, were used as the forced and natural convection Nusselt numbers, respectively, for all four variations on the 1-D heat transfer model.

*Model Variations.* Different model variations were considered with the understanding that few end-users would have the depth of information and measurements available through NIST's BIPV test bed. As shown previously in Table 4, Model 1 includes all available data from the test facility, and Model 4, for example, includes data that is expected to be available to all users. Table 9 compares  $R^2$  values between models for both panels.

Figures 5 and 6 show the panel temperatures predicted by the different model variations for the uninsulated and insulated panels, respectively. Model 1 predicts the operating temperature of both panels considerably better than the NOCT model. Figure 5 shows that the uninsulated panel temperatures are within 5 K throughout both the clear and cloudy days. This is an improvement over the 10 K underprediction of the NOCT model for an uninsulated panel. This improvement can be seen in the  $R^2$  value for Model 1 in Table 9. The predicted power, Tables 10 and 11, using the panel temperatures from Model 1 closely agree with the

power predicted using the measured panel temperatures, which corresponds to the closely matching temperatures predicted by the model.

The insulated panel temperatures are also more closely predicted using Model 1, Fig. 6, compared to the NOCT model. The proposed model overpredicts the panel temperatures during the midday. This overprediction may be the result of the one-dimensional heat transfer assumption in the insulated case. The thermal resistance of the insulation is so great that a significant amount of heat may be lost laterally to the aluminum framework supporting the panel. The overprediction of the panel temperatures results in an underprediction of the peak power using Model 1, as seen in Table 11. Also, Table 10 shows that the overprediction of temperatures by Model 1 results in a slight drop in the predicted energy production over the entire modeled period.

The first variation in the model (Model 2), which assumes that the temperature of the surroundings is equal to the respective ambient temperatures, results in a higher temperature prediction relative to Model 1. In general, the effective temperature of the outdoor surroundings is less than the outdoor ambient temperature. Therefore, the outdoor radiative heat transfer decreases with this assumption, and less heat transfer to the environment would drive the predicted panel temperatures higher.

Conversely, the second variation of the model (Model 3), which simplifies the model further by assuming that the wind speed measured on the roof equals the wind speed on the wall, works to improve the temperature predictions for both the insulated and uninsulated panel. The wind speed on the roof is significantly higher than the wind speed on the BIPV wall. Thus, the convective heat transfer at the outside surface is higher, which brings the temperatures down in both cases. The decrease in panel temperatures results in a higher predicted power, which improves the insulated predicted total energy production but makes the total energy prediction worse for the uninsulated case.

The majority of users will employ Model 4. This model uses measured horizontal radiation to approximate the solar radiation on a sloped surface, a vertical surface in the case of the NIST BIPV test bed. The irradiance transformation slightly underestimates the irradiance on a vertical surface for cloudy days.

The lower irradiance estimations in Model 4 lead to a cooler panel temperature prediction for both panels on cloudy days. The panel temperature predictions on clear days closely match those in the previous model. Similarly, the power prediction for cloudy days suffers due to the lower irradiance estimate, but on clear days, the peak power closely matches that of Model 3.

**Comparison of NOCT Model and Model 4.** Using the transformed horizontal irradiance measurements, the NOCT model and the fourth version of the one-dimensional heat transfer model start on an even plane. Figure 7 shows that Model 4 provides a better estimate of the panel temperatures for both insulated and uninsulated panels. Except for the partly cloudy day with the lower irradiance estimate, both the NOCT model and Model 4 closely predict the power output for the uninsulated panel, as

**Table 11 Predicted energy (kWh) and the percent difference from the predicted energy using the measured panel temperature for each panel on both a clear and cloudy day**

Source of Panel Temperatures	Uninsulated Panel Clear Day		Uninsulated Panel Cloudy Day		Insulated Panel Clear Day		Insulated Panel Cloudy Day	
	kWh	% Diff	kWh	% Diff	kWh	% Diff	kWh	% Diff
	Measured	0.296		0.191		0.277		0.182
Model 1	0.294	-0.7	-0.190	-0.6	0.270	-2.6	0.178	-2.4
Model 2	0.292	-1.4	0.190	-0.8	0.266	-4.1	0.176	-3.6
Model 3	0.297	0.2	0.191	0.0	0.278	0.1	0.180	-1.1
Model 4	0.294	-0.7	0.169	-11.8	0.275	-0.7	0.160	-12.1
NOCT-Measured Vertical Irradiance	0.307	3.6	0.196	2.5	0.307	10.6	0.196	7.7
NOCT-Predicted Vertical Irradiance	0.304	2.6	0.173	-9.6	0.304	9.6	0.173	-5.0

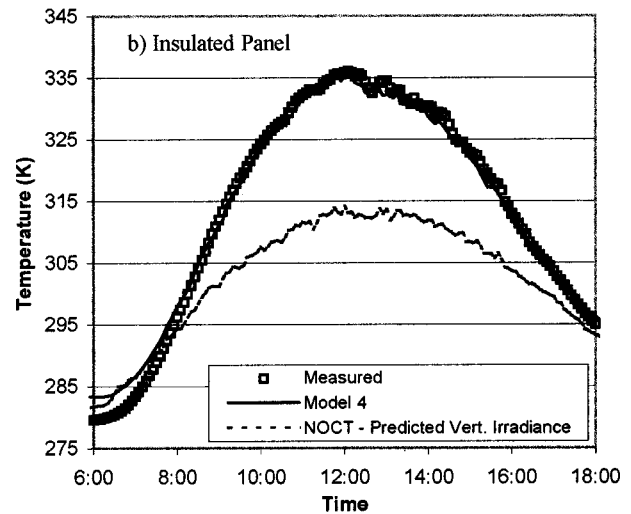
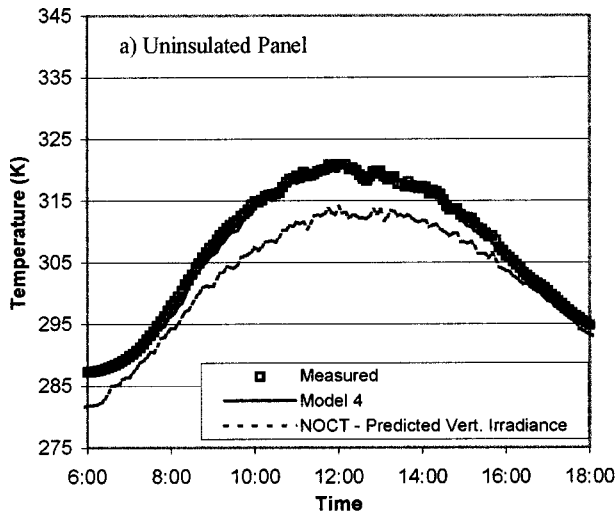


Fig. 7 Comparison panel temperatures predicted by NOCT model using the estimated vertical irradiance and Model 4 for an (a) uninsulated panel on a clear day, and (b) insulated panel on a clear day

shown in Table 11. However, the NOCT model greatly overpredicts the power for the insulated case. This clearly shows the limitations of the NOCT model. The NOCT model does not have the ability to adjust to the different mounting scenarios; it predicts the exact same power for both the insulated and uninsulated panels.

## Conclusions

The NIST BIPV test facility provides high-quality experimental data for the validation of predictive performance tools. The NOCT model is widely used to estimate panel temperatures, but the data recorded at NIST indicates that the NOCT model consistently underpredicts the panel temperatures, and the actual panel temperatures can be as much as 20 K higher than the predictions of the NOCT model for an insulated panel. A more complex, one-dimensional heat transfer model was derived to improve upon the NOCT model. Forced and natural convection relations were chosen from 8 combinations, and four variations of the model were investigated. Model 1 included measurements not readily available to most building designers, but it was the most realistic. Model 4 only included variables that are accessible by the majority of designers. All of the models reasonably predicted the panel temperatures for both insulated and uninsulated panels. When compared to the NOCT model, Model 4 more accurately modeled the panel temperatures, especially for insulated panels.

## Appendix A

The uncertainties of the measured quantities used to evaluate the one-dimensional and NOCT models in this paper are shown in Table A1.

Table A1. Expanded uncertainties of measured quantities

Quantity	Expanded Uncertainty ( $k=2$ )
$T_{\text{cell}}$	0.24°C
$T_{\text{ambient}}$	0.24°C
$T_{\text{surr}}$	1.50°C
$T_{\text{surr,indoor}}$	1.50°C
$G_{\text{total}}$	12.0 W/m <sup>2</sup>
$G_{\text{beam}}$	12.0 W/m <sup>2</sup>
$V$	0.27 m/s
Peak Power	0.48 W

Table A2. Instrument uncertainties

Instrument	Uncertainty (Type)
Thermocouple	0.09°C (A)
Thermometers	0.03°C (B)
PSP	0.5% (B)
NIP	0.5% (B)
PIR	1.0% (B)
Anemometer	0.135 m/s (B)
DVM	0.005% of reading + 0.004% of full scale (B)

These expanded uncertainties were calculated using the law of propagation of uncertainty and a coverage factor of 2 ( $k=2$ ). The uncertainty of the thermocouples used to measure  $T_{\text{cell}}$  and  $T_{\text{ambient}}$  was determined statistically from a calibration performed with NIST calibrated thermometers. The uncertainties of all other instruments were assumed from manufacturer's specifications. All uncertainties reported by a manufacturer that did not include a coverage factor were assumed to incorporate a coverage factor of 1 ( $k=1$ ). The instrument uncertainties are listed in Table A2.

## Nomenclature

### Uppercase

$G$	= solar irradiance (W/m <sup>2</sup> )
$G_{\text{effective}}$	= effective irradiance on a BIPV panel (W/m <sup>2</sup> )
$Gr$	= Grashoff number
$H$	= height of panel (m)
$L$	= thickness (m)
NOCT	= nominal operating cell temperature (K)
$\bar{Nu}$	= average Nusselt number
$P$	= perimeter of panel (m)
$Pr$	= Prandtl number
$Re$	= Reynolds number
$R^2$	= correlation coefficient
$T$	= temperature (K)
$V$	= velocity (m/s)
$W$	= width of panel (m)
Zenith	= elevation of sun in sky (degrees)

## Lowercase

- day = integer day of the year (1–365)  
 $\bar{h}$  = average convective heat transfer coefficient (W/m<sup>2</sup> K)  
 $k$  = thermal conductivity (W/m K)  
 $n$  = index of refraction  
 $q''$  = heat flux (W/m<sup>2</sup>)  
 $t$  = time (s)

## Greek

- $\alpha$  = solar absorptance of the PV cell  
 $\beta$  = slope of panel (degrees)  
 $\Delta t$  = length of time step (s)  
 $\varepsilon$  = emissivity  
 $\eta_o$  = average efficiency of PV cell  
 $\theta$  = incident angle of sun on panel (degrees)  
 $\rho$  = density (kg/m<sup>3</sup>)  
 $\tau(\theta)$  = solar transmittance as a function of the incident angle

## Subscripts

- conv = heat flux due to convection  
Hor = irradiance on a horizontal surface  
 $i$  = material indicator (glass, PV cells, backsheet, or insulation)  
in = inside  
NOCT = nominal operating cell temperature  
NIP = measured by a normal incidence pyrheliometer  
out = outside  
PIR = measured by a precision infrared radiometer  
PSP = measured by a precision spectral pyranometer  
rad = heat flux due to radiation

- s = surface  
st = heat flux due to energy storage  
surr = surroundings  
total = net irradiance

## References

- [1] "1999 PV Module, Cell Shipments Break Record, Reaching 77k Peak Kilowatts," *Solar Renewable Energy Outlook*, 2000, **26**, No. 16, p. 182.
- [2] ASTM, "E 1036M Standard Test Methods for Electrical Performance of Non-concentrator Terrestrial Photovoltaic Modules and Arrays using Reference Cells," *Annual Book of ASTM Standards*, Vol. 12.02.
- [3] Fanney, A. H., and Dougherty, B. P., 2000, "Building Integrated Photovoltaic Test Facility," *Proc. of ASES, NPSC, AIA, ASME, MREA Conf. Solar 2000*.
- [4] Fanney, A. H., Dougherty B. P., and Davis, M. W., 2001, "Measured Performance of Building Integrated Photovoltaic Panels," *Proc. of Forum 2001, Solar Energy: The Power to Choose*, April 2001, ASES, Washington, DC.
- [5] King, D. L., 1997, "Photovoltaic Module and Array Performance Characterization Methods for All System Operating Conditions," *Proc. of NREL/SNL Photovoltaics Program Review Meeting*, AIP Press, New York.
- [6] Duffie, J. A., and Beckman, W. A., 1991, *Solar Engineering of Thermal Processes*, John Wiley and Sons, New York.
- [7] [http://www.siemenssolar.com/sp75\\_sp70.html](http://www.siemenssolar.com/sp75_sp70.html)
- [8] Matz, E., Appelbaum, J., Taitel, Y., and Flood, D. J., 1997, "Solar Cell Temperature on Mars," *J. Propul. Power*, **14**, No. 1, pp. 119–125.
- [9] AFG Manufacturer's Specification Sheet, Krystal Clear Glass.
- [10] Siemens, Manufacturer's Cell Specification Sheet.
- [11] Incropera, Frank P., and DeWitt, David P., 1996, *Fundamentals of Heat and Mass Transfer*, 4th edition, John Wiley and Sons, New York.
- [12] Parretta, A., Sarno, A., Tortora, P., Yakubu, H., Pasqualino, M., Zhao, J., and Wang, A., 1999, "Angle-Dependant Reflectance Measurements on Photovoltaic Materials and Solar Cells," *Opt. Commun.*, **172**, pp. 139–151.
- [13] E. I. DuPont, General Properties Specification, Tedlar<sup>®</sup>
- [14] E. I. DuPont, Physical-Thermal Properties Specification, Mylar<sup>2</sup>
- [15] Kays, W. M., and Crawford, M. E., 1993, *Convective Heat and Mass Transfer*, McGraw Hill, New York.
- [16] Wolfe, W. L., and Zissis, G. J., (eds.), 1989, *The Infrared Handbook*, Office of Naval Research, Department of the Navy, Washington, DC.